Mesovortex Circulations Seen by Airborne Doppler Radar within a Bow-Echo Mesoscale Convective System

David P. Jorgensen and
Bradley F. Smull
NOAA/NSSL/Mesoscale
Research Division,
Boulder, Colorado

Abstract

During the spring of 1991, scientists from the National Severe Storms Laboratory conducted a field observational program to obtain a better understanding of the processes responsible for organizing and maintaining the dynamical and electrical structure of mesoscale convective systems (MCSs), as well as mechanisms acting to organize and propagate the dryline. Extensive use was made of a relatively new observing tool, the airborne Doppler radar installed on one of the NOAA P-3 research aircraft, to map the precipitation and kinematic structure of large mesoscale convective systems. The radar was operated in an innovative scanning mode in order to collect pseudo-dual-Doppler wind data from a straight-line flight path. This scanning method, termed the fore/aft scanning technique (FAST), effectively maps out the three-dimensional wind field over mesoscale domains (e.g., 80 km x 100 km) in ~15 min with horizontal data spacing of 1–2 km. Several MCSs were observed over central Oklahoma during May and June of 1991, and one such system exhibiting a "bow-echo" structure is described. Many observed features of this MCS correspond to structures seen in nonhydrostatic numerical simulations. These features include a pronounced bulge or "bow" in the convective line (convex toward the storm's direction of propagation), a strong descending rear inflow jet whose axis is aligned with the apex of the bow, and a cyclonic vortex (most pronounced at heights of 2–3 km) situated in the trailing stratiform region lateral to the axis of strongest rear inflow. Doppler-derived wind analyses reveal the likely role played by the mesoscale circulation in twisting environmental vertical shear and converging ambient vertical vorticity in maintaining and amplifying the vortex. The relatively detailed yet horizontally extensive airflow analyses also reveal the utility and advantages of airborne Doppler radar in the study of large convective systems.

1. Introduction

"Bow-echo"-type mesoscale convective systems (MCSs) have long been identified by their distinctive radar echo pattern as a 50–100-km-long bow-shaped segment of rapidly advancing convective storms (Fujita 1978), with the apex of the bow pointed toward the direction of advance. The most severe of these systems, which have been termed "derechos" (a Spanish term meaning "straight ahead"), produce long swaths of damaging, straight-line surface winds (Johns and Hirt 1987; Przybylinski and Gery 1983). Recent numerical simulations by Weisman (1992) indicate that bow-echo MCSs possess a unique dynamic structure, embodying a strong "rear-inflow" jet extending to the leading edge of the bow and descending to near the surface. Model sensitivity tests indicate that the development of this structure requires large amounts of convective available potential energy and strong ambient environmental vertical wind shear sufficient to establish deep forced ascent of low-level air at the leading edge. Johns et al. (1990) demonstrated that such conditions are frequently observed in advance of the severe bow echoes. The numerical results of Weisman also indicate that the rear-inflow jet is essential for the maintenance of the convectively generated cold pool along the leading edge and hence the forced lifting of low-level air ahead of the system. Such circulation features have recently been seen in Doppler radar observations of bow echoes (Schmidt and Cotton 1989; Burgess and Smull 1990).

An interesting aspect of Weisman's simulations is the existence in the mature phase of the system of "bookend" vortices on the flanks of the convective line, with the cyclonic gyre located at the north end of the line, with an anticyclonic gyre on the southern end. The existence of midlevel convectively generated vortices has been known for some time (e.g., Houze et al. 1989) and is usually most evident in the decaying phase of MCSs (Bartels and Maddox 1991). To date, however, limited observations have been available to document vortex structure in mature bow-echo convective systems.

During the spring of 1991, the National Severe Storms Laboratory (NSSL) of the National Oceanic and Atmospheric Administration (NOAA) conducted a field project called COPS-91 (Cooperative Oklahoma Profiler Studies) to gather data using a variety of sensors (e.g., instrumented aircraft, surface mesonet stations, ground-based Doppler radars, wind profilers, and mobile sounding systems capable of profiling both standard meteorological and electrical conditions) in

©1993 American Meteorological Society

mesoscale convective systems over central Oklahoma and along the dryline in the Texas Panhandle. Extensive use was made of the NOAA P-3 aircraft in COPS-91, particularly its vertically scanning, X-band airborne Doppler radar. The principal advantages of an airborne Doppler radar over installation of a ground-based dual-Doppler network are twofold: 1) potential uncertainties due to scanning geometry can be minimized because the chief scientist can usually specify flight tracks that maximize data coverage, and 2) the aircraft is generally more cost effective as many more meteorological cases can usually be sampled (i.e., the ability to go to the weather rather than waiting for the weather to come through the ground-based dual-Doppler network). In some situations, such as over the remote oceans, airborne Doppler radar is the only practical means of documenting MCS structure, as evidenced by the success of the recently completed Tropical Ocean–Global Atmosphere Coupled Ocean Atmosphere Response Experiment (TOGA/COARE). In TOGA/COARE three Doppler equipped turboprop aircraft—two NOAA P-3s and the Lockheed Electra operated by the National Center for Atmospheric Research (NCAR)—combined for 77 flight sorties in a 4-month period. The primary limitation of the airborne radar lies with its rather limited endurance compared to the typical life cycle of an MCS. The nominal 10-h flight duration of the P-3s often limits data coverage to a few snapshot looks at mature system structure.

On two occasions during COPS-91, the NOAA P-3 aircraft equipped with a vertically scanning, X-band Doppler radar intercepted bow-shaped convective systems. Analysis of those data reveals the existence of mesoscale vortices in the trailing stratiform region of mature convective systems, bearing a strong resemblance to the simulations of Weisman (1992). Companion papers by Marshall and Rust (1993) and Hane et al. (1993) describe the electrical structure of several of these convective systems and dryline morphology, respectively. The characteristics of the airborne Doppler radar including its scanning methodology are described in section 2. In section 3 we show analyses of structure and airflow in the 8 May 1991 MCS. A possible mechanism for the generation and maintenance of the trailing region mesovortex is discussed in section 4.

2. Description of the airborne Doppler radar

The Doppler radar installed on the NOAA P-3 is described in detail in Jorgensen and DuGranrut (1991). The radar is a vertically scanning, X-band (3.2-cm wavelength) Doppler radar mounted near the tail of the P-3. The basic scanning methodology is schematically illustrated in Fig. 1. This scanning procedure—first proposed by Frush et al. (1986) and later elaborated by Hildebrand (1989) for use by the airborne Doppler radar proposed for the Electra aircraft [ELDORA (Electra Doppler Radar)] operated by the National Center for Atmospheric Research—consists of collecting two scans of data: one pointing ~25° forward from a plane normal to the flight track, and one scan pointing aft ~25°. This technique is termed the fore/aft scanning technique (FAST). As the aircraft moves in a quasi-straight flight path, FAST scans sweep out a three-dimensional region of space surrounding the aircraft's track. If the antenna is rotated at its maximum rate of 10 rpm (60° s^{-1}), at typical P-3 ground speeds (~120 m s^{-1}) adjacent beams intersect with horizontal spacing of ~1.5 km. An improvement in the horizontal data spacing to ~750 m can be obtained if the antenna is scanned in a sector confined to one side of the track. The increase in data density comes at the expense of the areal coverage on both sides of the track. Where two beams intersect an estimate of the horizontal wind velocity can be obtained using the methods described in Jorgensen and DuGranrut (1991). Vertical velocity is then obtained by downward (or upward) integration of the equation of continuity subject to boundary conditions of zero vertical air motion near the surface and echo top, using an O'Brien (1970) correction to the divergence profile.

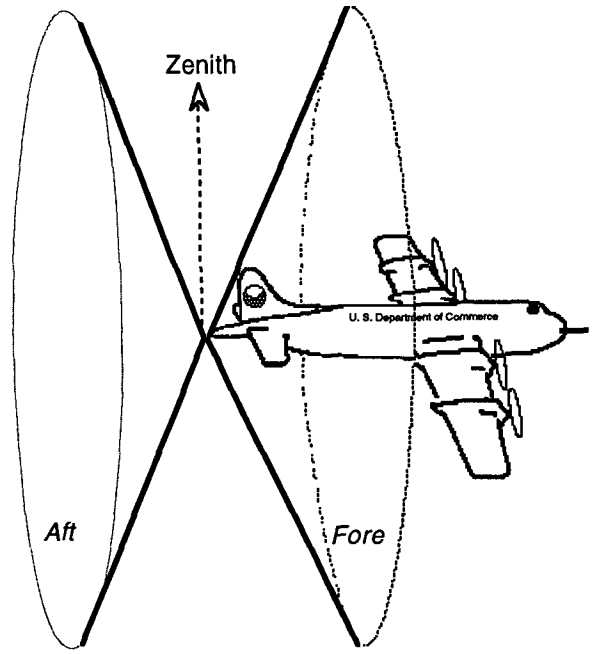

FIG. 1. Schematic illustration of the P-3's tail-mounted Doppler radar scanning geometry. Alternate sweeps of the vertically scanning antenna point ± 25° forward and aft of a plane normal to the aircraft's longitudinal axis.

Although the radar signal is digitized out to a maximum range of 76 km, the 1.9° vertical beamwidth of the radar limits the practical maximum range to about 50 km because of beam spreading.

Prior to the synthesis of the horizontal winds, the radial velocity induced by the aircraft's motion must be subtracted from the Doppler radar data. Assuming a fore/aft-looking angle of ±25° and ground speed of 120 m s^{-1}, nearly 50 m s^{-1} of aircraft motion is induced into the radial velocity observations. This contribution is the same for all range gates along a given beam and is subtracted out to produce a velocity estimate that is accurate to ~1.5 m s^{-1} (Jorgensen et al. 1983). Other radial velocity artifacts induced by improper antenna pointing (revealed by residual motion in the ground return) are removed as well. The radial velocity must also be dealiased for velocity ambiguities due to the relatively small Nyquist velocity interval of ±12.9 m s^{-1}.

3. Observations and analyses of the 8 May 1991 bow-echo convective system

The evolution of the radar pattern of this MCS is shown in Fig. 2. During the late afternoon of 7–8 May 1991 (about 2300 UTC 7 May 1991), strong convective storms developed along the dryline in the central Texas Panhandle coincident with the approach of a 500-mb short-wave trough (Fig. 3a). Though initially isolated, convection rapidly evolved into an ~100-km-long north–south line of storms and began propagating eastward. By about 0600 UTC 8 May, the convective line had traversed the western half of Oklahoma. The convection dissipated in central Oklahoma after 0600 UTC, but a large region of stratiform precipitation remained over central Oklahoma until about 1200 UTC. The morning 500-mb chart valid at 1200 UTC (Fig. 3b) reveals a pronounced sharpening of the trough over western Oklahoma. In spite of the approaching trough axis, the expected height *fall* of 20 m at Norman (in central Oklahoma) was accompanied by a 4°C *rise* in the 500-mb temperature. As we will demonstrate, this peculiar signature was likely related to the presence of an MCS-induced mesovortex over southwest Oklahoma.

a. Structure of the leading convective line and its rear inflow

Apparent from 0200 UTC to about 0500 UTC in Fig. 2 is a pronounced eastward "bulge" in the convective line, most noticeable near the Texas–Oklahoma border (Red River). During this period, the convective line moved eastward at about 13 m s^{-1}, with the apex of the bow tracking along the Red River. To the rear (i.e., west) of the convective line was a region of largely stratiform rainfall identified by an extensive "bright band" of enhanced radar reflectivity near the melting level [~3.5 km above ground level (AGL)]. After 0500 UTC, the Texas portion of the convective line plunged rapidly southeastward, while the Oklahoma segment (which was the focus of more detailed observations) both slowed and weakened. In Oklahoma, the band of heaviest stratiform precipitation moved somewhat slower than the convective line (~9 m s^{-1} versus 13 m s^{-1}) and more toward the southeast. An echo-free "notch" developed at the back edge of the stratiform echo over southwest Oklahoma and was associated with a wake low in the surface pressure field as seen in both observations (Johnson et al. 1989) and simulations (Zhang et al. 1989) of other MCSs. A cyclonically curved, hooklike appendage that developed on the north side of the notch (cf. 0500–0700 panels in Fig. 2) strongly suggests the presence of a mesovortex, as shown by Johnson and Bartels (1992). Confirmation of such a circulation, however, hinges on more detailed data provided by the P-3 aircraft.

Between 0500 UTC and 0900 UTC, the P-3 flew a combination of northwest–southeast tracks parallel to the rear edge of the convective line and east–west legs across the stratiform notch region. Data from the P-3's vertically scanning Doppler radar were collected during much of this period. The horizontal projection of the pattern of intersecting fore- and aft-looking radar beams for a portion of the flight into the 8 May convective system is shown in Fig. 4. As the aircraft traversed the region immediately behind (i.e., west of) the principal convective line, a domain spanning the full depth of the troposphere over a horizontal region of 80 km x 100 km was swept out in about 18 min.

The horizontal wind field relative to the slower-moving stratiform rain region at 2.5 km AGL derived from the P-3's initial pass behind the convective line (0509–0533 UTC) is presented in Fig. 5. The domain of this analysis is shown relative to the broad reflectivity pattern by the region of cross-hatched beams immediately west of the convective line in Fig. 2. At its southern end, the flight track neared the apex of the bowing convective line. Winds at this level are primarily from the west, although southerly flow is seen in the northern part of the domain behind the weakening portion of the line. Toward the south, winds shift to the west-northwest and markedly strengthen. The core of this rear inflow (exceeding 20 m s^{-1} in ground-relative terms) is located immediately behind the pronounced bow in the convective line. Although speeds dropped below 2.5 km, individual Doppler vertical sweeps (not shown) indicate this rear inflow descended toward the convective line and helped sustain the strong westerly

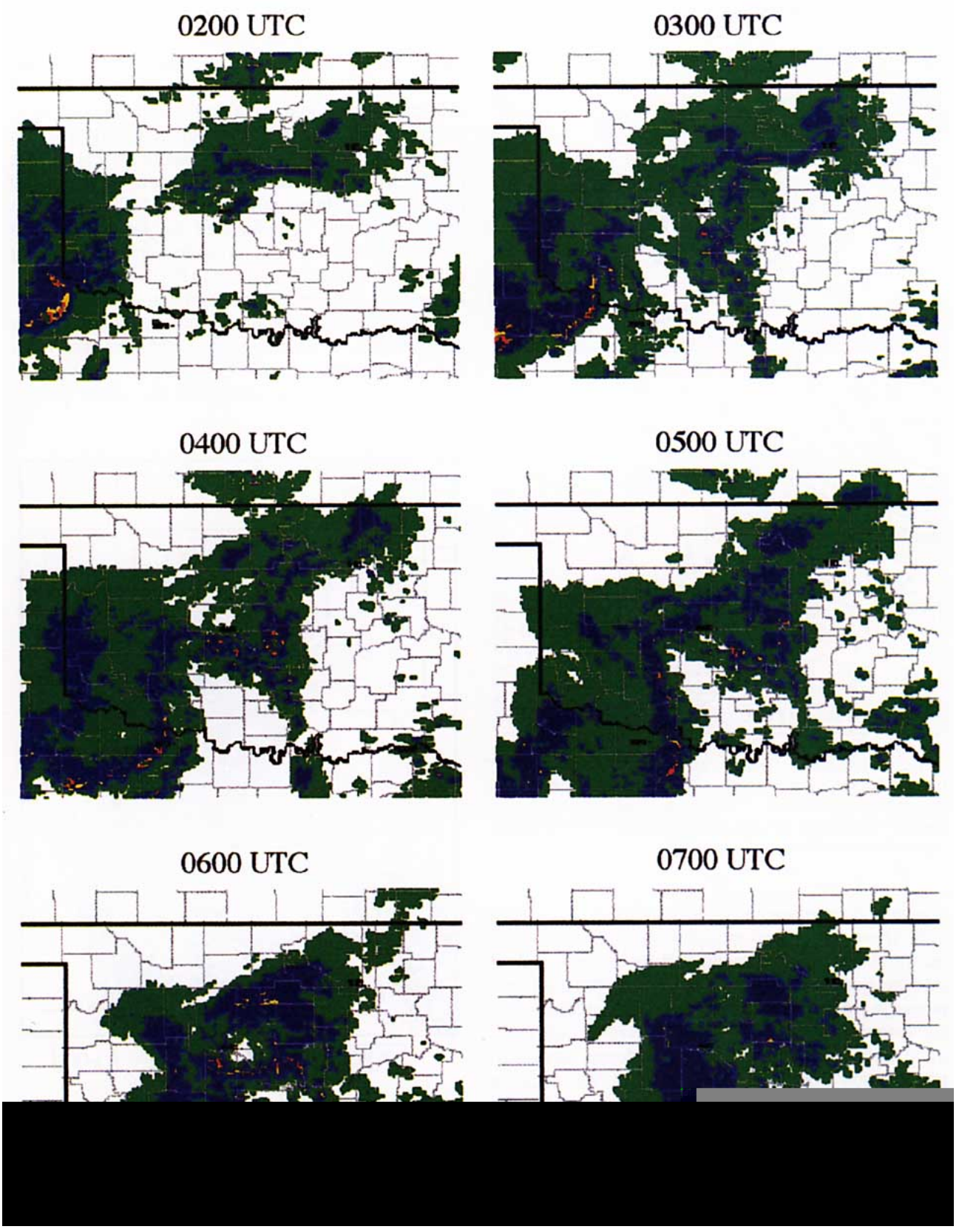

FIG. 2. Composite low-level radar reflectivity patterns showing the evolution of the bow-echo convective system at hourly intervals beginning at 0200 UTC 8 May 1991. Shading indicates precipitation echo intensity according in equivalent radar reflectivity units (dB*Z*) according to the following scale: green: 18–30 dB*Z*; blue: 30–41 dB*Z*; yellow: 41–46 dB*Z*; and red: >46 dB*Z*.

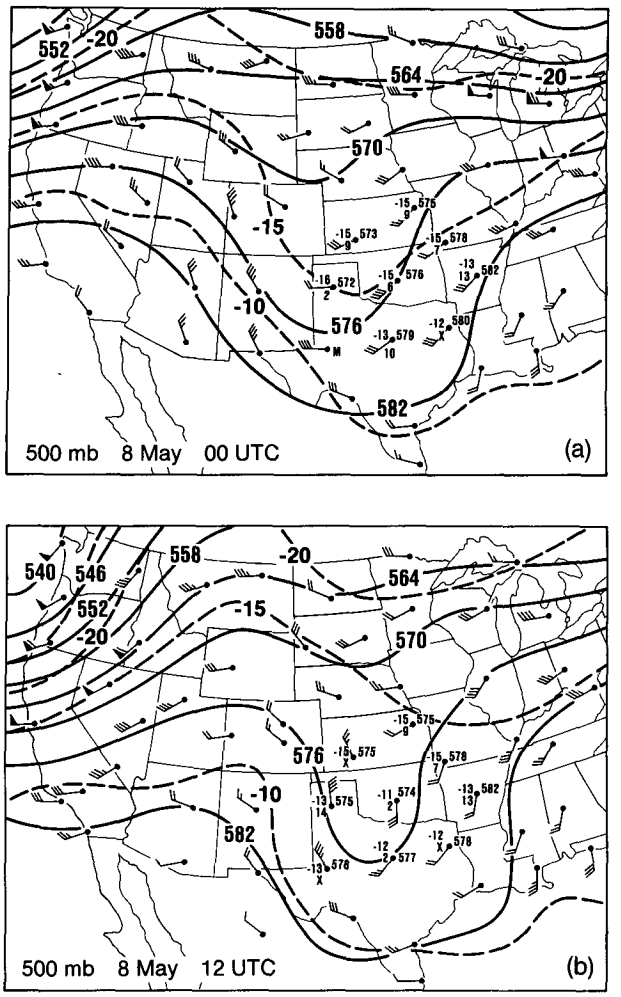

FIG. 3. NMC 500-mb analyses for (a) 0000 UTC and (b) 1200 UTC 8 May 1991. Solid contours are geopotential height (dm), while dashed lines are isotherms (°C). Observed values of temperature, dewpoint depression, and geopotential height are restricted to the region of special interest.

low-level flow immediately west of the surface gust front. (No damage was reported, but surface winds of up to 15 m s^{-1} were measured by NSSL's mobile laboratory in west-central Oklahoma during gust front passage.) A narrow zone of cyclonic curvature and convergence coincides with a narrow reflectivity minimum separating the region of moderate stratiform precipitation from the convective line, but cyclonic shear/curvature are evident on a broader scale behind the north end of the convective line (upper-left portion of Fig. 5).

b. Vortex structure in the trailing stratiform region

Mesoscale vortices within the trailing stratiform rain region of some MCSs have been documented in many earlier studies (e.g., Smull and Houze 1985; Houze et al. 1989; Brandes 1990; Bartels and Maddox 1991; Biggerstaff and Houze 1991; Johnson and Bartels 1992). These vortices, thought to be induced and maintained by convergence of planetary and preexisting vertical relative vorticity and mesoscale twisting of environmental shear by differential vertical motion, typically are seen at low- to midtropospheric levels in the trailing stratiform regions of mature and dissipating MCSs. Vortices have also been seen in simulated convective systems (Zhang et al. 1989; Weisman 1992). Recently, Brandes and Ziegler (1993) have shown the importance of downdraft-induced twisting of horizontal vorticity inherent to the descending rear-inflow circulation in generating these vortices.

Although a complete vorticity budget (i.e., one illustrating the relative importance of various production and advection terms for the MCS and its near environment) is not possible due to the lack of a dense

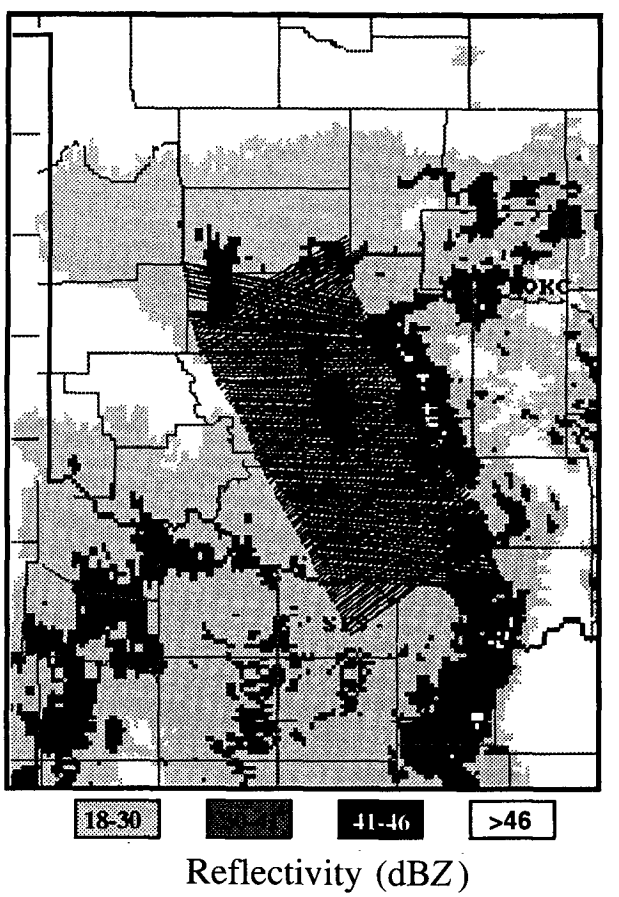

FIG. 4. Composite low-level radar reflectivity pattern at 0515 UTC 8 May 1991 centered on Oklahoma (superimposed heavy state outline) constructed from National Weather Service radars at Oklahoma City, Oklahoma (OKC); Tulsa, Oklahoma (TUL); and Wichita Falls, Texas (SPS). The cross-hatched pattern to the west of the principal convective line represents the horizontal projection of the airborne Doppler radar's scans during the period 0509 UTC to 0533 UTC. The P-3 flight track is shown by the dashed line near the center of the cross-hatched pattern.

sounding network, airborne Doppler data does reveal kinematic conditions *within* the trailing stratiform region of the 8 May convective system. In spite of the superior coverage afforded by an airborne radar platform, a composite of several tracks flown across the stratiform region is required to document the full breadth of this circulation. Figure 6 shows the 2.5-km AGL flow pattern relative to the moving stratiform region over a 200-km x 160-km composite analysis, which allowed for movement of the stratiform echo during the ~3-h period spanned by these observations (from 0600 UTC to 0840 UTC). Note that this analysis encompasses the hook-like stratiform echo appendage previously noted at 0700 UTC in Fig. 2. The flow pattern evinces profound cyclonic vorticity ($\geq 2 \times 10^{-4}$ s^{-1}) on a scale of ~100 km. The circulation was most pronounced at 2.5 km but was evident in the Doppler radar data up to 5 km. In the eastern half of the domain, the flow is southerly but abruptly shifts to northerly within the curved echo appendage to the west. Lack of radar return in the notch region limits the Doppler wind analysis; a complementary depiction of the mesovortex is provided by extracted from two east–west passes (shown as dashed lines in Fig. 6) at the ~3.2-km flight level somewhat later in the mission (Fig. 7). Cyclonic vorticity is clearly seen. Easterly flow encountered on the southernmost track (which extended across the notch) providing evidence of a closed circulation. Southerly flow carried relatively high θ_e (equivalent potential temperature) values, identifying air that had recently emerged from the convective line over Texas. To the west, lower θ_e values were associated with drier environmental air entering the rear of the system. A relative minimum in θ_e was seen near the center of the circulation. Because equivalent potential temperature typically decreases with height to a relative minimum at midlevels, the presence of lower values near the center implies locally intense descending motion. A mesoscale downdraft to the rear of the stratiform region is also consistent with the "notch" pattern in the radar reflectivity composite of Fig. 4, since descending motion would promote hydrometeor evaporation and thus a reduction of reflectivity.

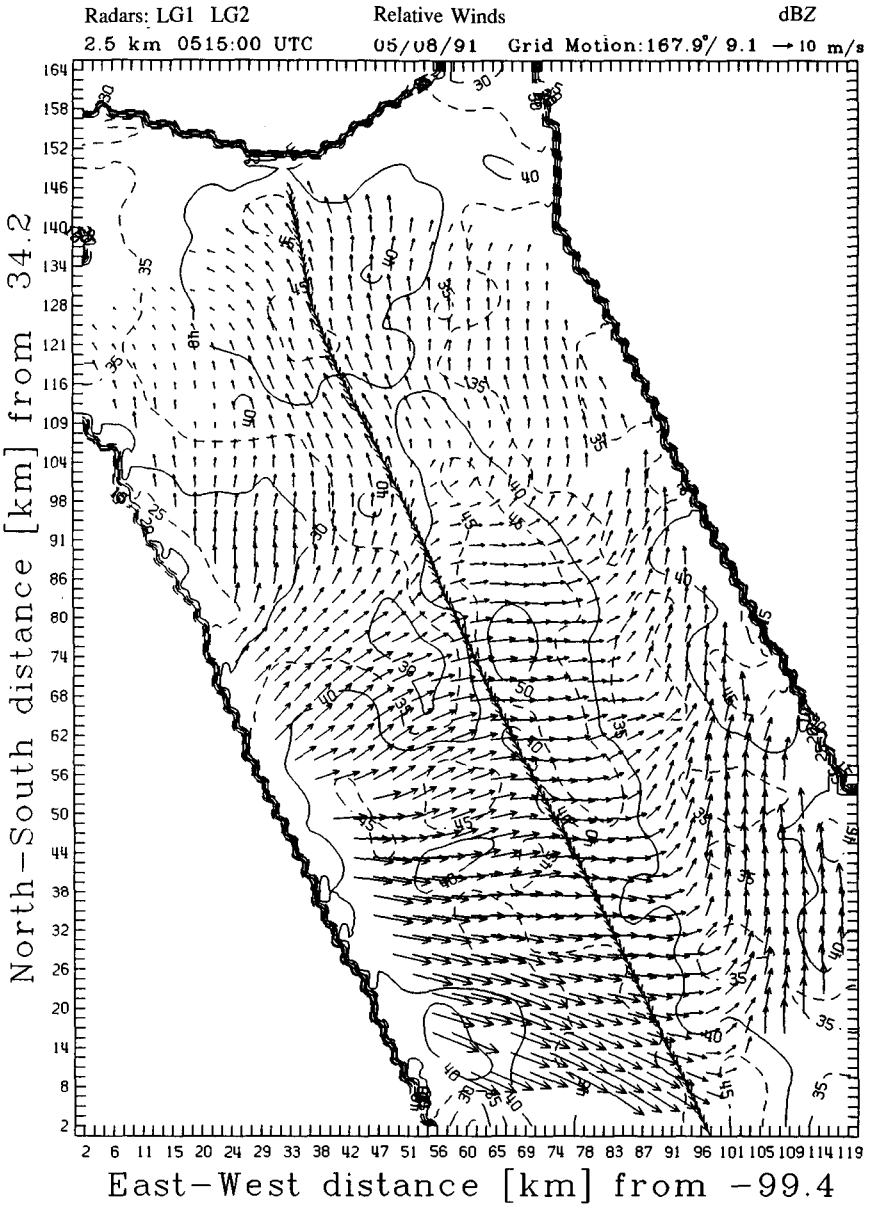

FIG. 5. Ground-relative wind field at 2.5 km AGL at 0509 UTC 8 May 1991 for the region just west of the convective line constructed from the P-3's Doppler radar data using the fore/aft scanning method. Flight track is the solid line with small arrows at 1-min intervals along the flight path. The scale for the wind vectors is shown in the upper right corner of the figure. Contours are X-band radar reflectivity in dBZ. The domain is 120 km x 165 km. Although the Doppler wind data were constructed on a 1.5-km x 1.5-km horizontal x 1-km vertical grid, wind vectors are plotted every 3 km for clarity.

Further evidence of a mesoscale downdraft within

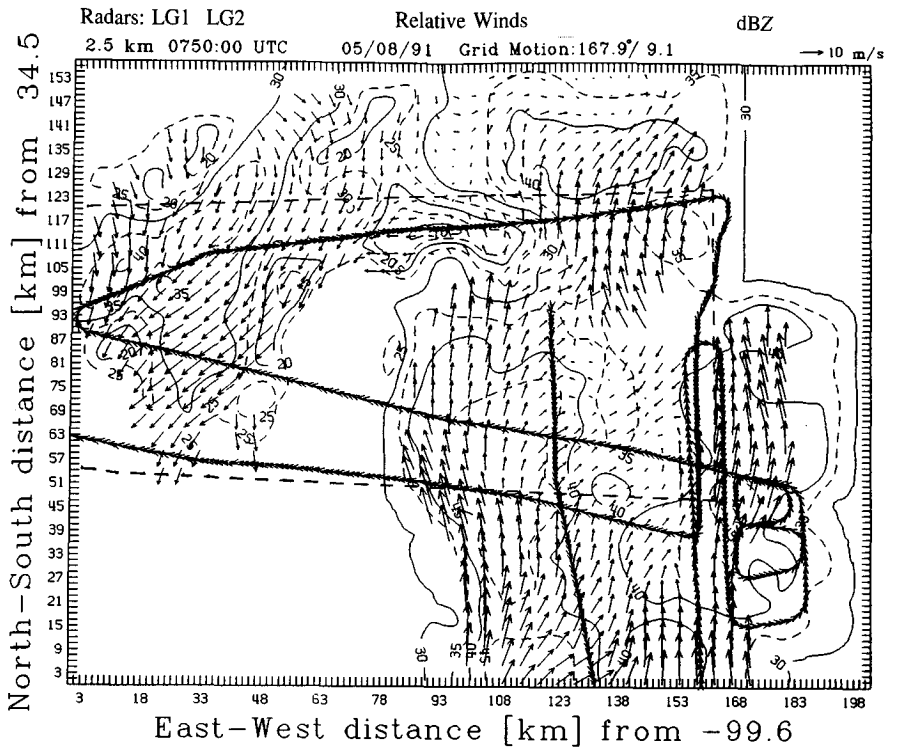

FIG. 6. As in Fig. 5 except at 2.5 km AGL over a 200 km x 160 km composite analysis domain fully encompassing the trailing mesovortex. The P-3 flight track over the period of the composite analysis (0600–0840) is shown by solid line with small arrows at 1-min intervals. The dashed line shows the P-3 track for the analysis shown in Fig. 7.

the trailing region can be seen in a sounding taken earlier from Amarillo, Texas (AMA), when the convective line was about 100 km to the east (Fig. 8). The sounding in Fig. 9 exhibits the classic "onion-shaped" profile, with highly subsaturated conditions below about 520 mb indicative of subsidence. Below the base of the trailing anvil, the wind profile shows strong westerly winds (~25 m s^{-1}), whose speed exceeded that of the MCS's precipitation region and thus constituted system-relative rear inflow. Westerly momentum did not extend to the surface but rode above the near-surface inversion at 810 mb. This inversion is characteristic of cool, moist outflow found in the wake of convective-scale downdrafts within intense squall lines.

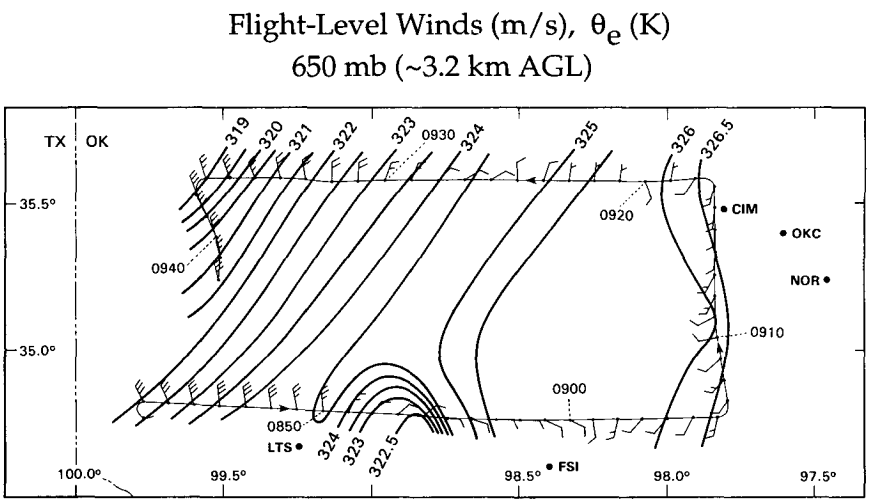

FIG. 7. The P-3 flight track at 650 mb (~3.2 km AGL) between 0843 and 0945 UTC. State borders are shown as dash-dotted lines. Ground-relative winds are plotted, with a full barb equal to 5 m s^{-1}. Numbers plotted at intervals along the flight track are equivalent potential temperature (q_e, K). Time marks are shown along the flight track at 10-minute intervals.

4. Possible processes contributing to the generation of the northern vortex

Vertical vorticity can be generated in an initially nonrotating atmosphere by tilting the horizontal vorticity inherent in the vertical shear of the ambient flow (Davies-Jones 1984; Rotunno and Klemp 1985). For example, cyclonic/anticyclonic circulation couplets are frequently seen in strong thunderstorms due to deformation of horizontal vortex lines on the flanks of updrafts embedded in strongly sheared flow. Once created, vertical vorticity can be amplified by stretching (convergence) of air into updrafts or downdrafts. Vorticity generation in supercell storms is recognized as fundamental to the process of storm splitting. Analogous processes of tilting and stretching may act on larger scales to produce counterrotating vortices at either end of strong convective lines. In Weisman's (1992) simulations of eastward-propagating bow echoes, a pair of bookend vortices developed, with cyclonic and anticyclonic circulations appearing near the northern and southern ends of the convective line, respectively. These simulated vortices initially developed in conjunction with

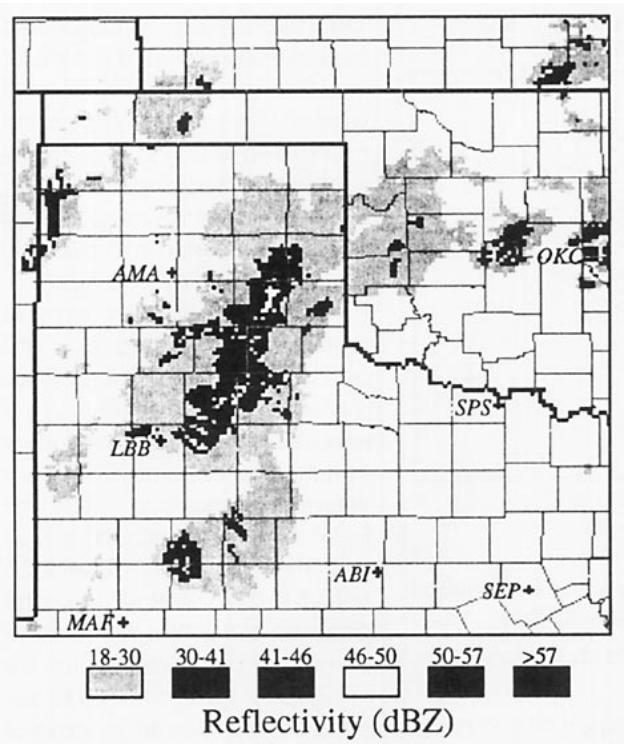

FIG. 8. Composite low-level radar reflectivity at 0000 UTC 8 May 1991. Shading indicates precipitation echo intensity according to the legend in Fig. 2. The location of the sounding in Fig. 9 is at Amarillo, Texas (AMA).

convective-scale storm splitting but amplified and expanded as the bow echo matured. Although a complete evaluation of the mechanisms acting to produce vertical vorticity in the trailing stratiform region cannot be accomplished with the present data (such a calculation would involve evaluating forces acting to produce spin along parcel trajectories extending into the nonprecipitating environment), a qualitative evaluation of the roles of tilting and stretching can be shown from the airborne Doppler analyses and environmental soundings.

To isolate the processes leading to vorticity amplification, we express the absolute vorticity tendency in a coordinate system following a parcel:

$$\frac{d}{dt}(\zeta+f) = \underbrace{-(\zeta+f)\left(\frac{\partial u}{\partial x}+\frac{\partial v}{\partial y}\right)}_{\text{convergence}} \underbrace{-\left(\frac{\partial w}{\partial x}\frac{\partial v}{\partial z}-\frac{\partial w}{\partial y}\frac{\partial u}{\partial z}\right)}_{\text{twisting}}, \quad (1)$$

where u, v, and w are the customary east–west, north–south, and vertical velocity components, respectively; ζ is the relative vorticity ($\zeta=\partial v/\partial x-\partial u/\partial y$); and f is the Coriolis parameter. In this form, the term labeled "convergence" represents the amplification of vertical vorticity by stretching of preexisting vertical vorticity by convergence associated with up or downdrafts, while the term labeled "twisting" represents the amplification due to tilting of vortex tubes in a vertically sheared environment. If the net tendency is toward increasingly cyclonic flow, then the two terms on the right side of (1) should sum to a positive value.

Horizontally averaged kinematic profiles to the rear of the convective line (computed over the Doppler analysis domain in Fig. 5) are shown in Fig. 10. The average relative vorticity (ζ) is slightly anticyclonic in the lowest 1 km, possibly a result of divergence at the base of the mesoscale downdraft. Cyclonic vorticity is maximized between 2 and 4 km, with values approaching 3×10^{-4} s^{-1}. Above 6 km the circulation is again anticyclonic, consistent with divergence atop a mesoscale updraft in the upper part of the stratiform cloud. The crossover between cyclonic and anticyclonic values occurs at about the same height as that between mesoscale ascent and descent (~6 km AGL). Mesoscale descent approaches –20 cm s^{-1} and fills the lower half of the troposphere, with weak mesoscale ascent above. A deep layer of convergence (owing to interaction of westerly rear inflow with more easterly flow emerging from the convective line) is found between 2 km and 8.5 km.

Coupled with the prevailing large-scale absolute

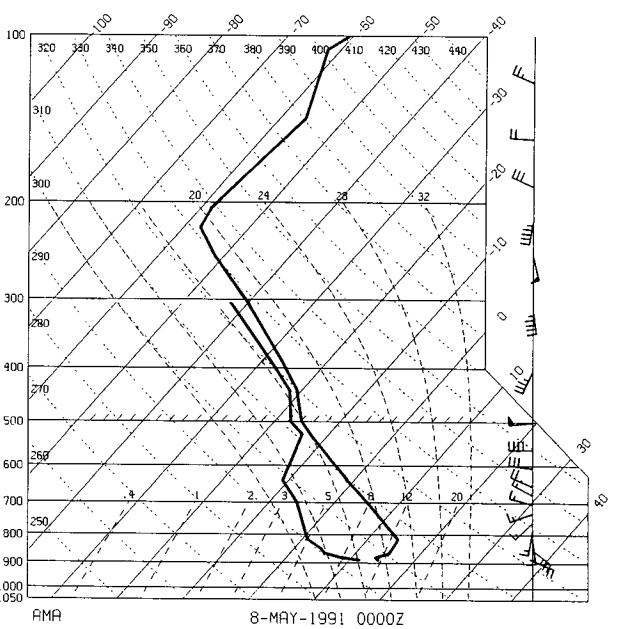

FIG. 9. Skew-T–log$p$ plot of the AMA sounding at 0000 UTC 8 May 1991 just to the west of the convective line. Wind barbs are meters per second with one full barb equal to 5 m s^{-1}.

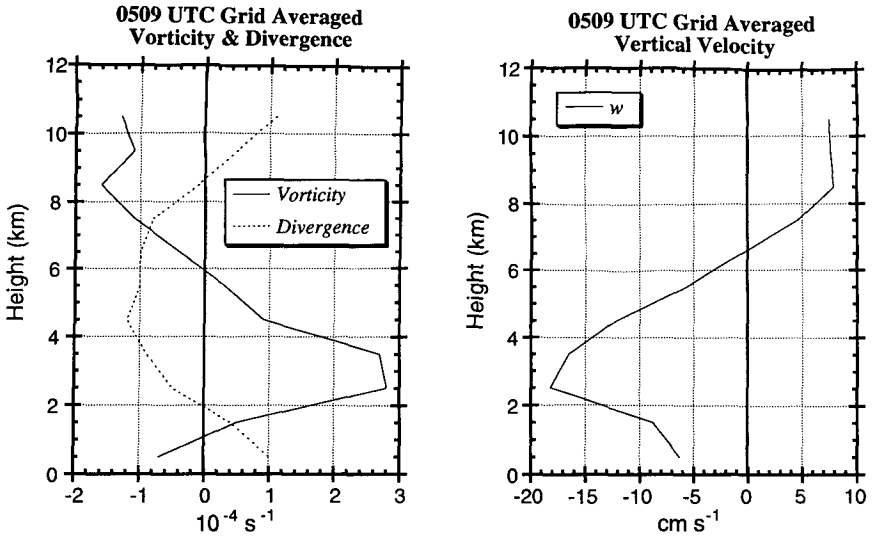

FIG. 10. Vertical profile of grid-mean relative vorticity and divergence (left panel) and vertical velocity (right panel) for the 0509 airborne Doppler-derived wind analysis of Fig. 5.

since subsidence warming would hasten evaporation of stratiform cloud and precipitation. Doppler wind analyses farther to the north (not shown here) indicate an absence of descending rear inflow, instead showing deep, weak ascent associated with easterly flow and embedded convection. Precise gradients in vertical motion are difficult to estimate due to lack of contiguous Doppler coverage; however, it is not unreasonable to assume that w switched sign northward from the axis of the rear inflow jet. Even assuming that the vertical velocity simply goes from –20 cm s^{-1} to zero over a horizontal distance of 100 km to the north of the jet axis yields a value for $\partial w/\partial y$ of ~2 x 10^{-6} s^{-1}. The corresponding vorticity generation rate due to twisting of ambient shear would be ~7 x 10^{-4} s^{-1} day^{-1}, which is roughly equivalent to the rate of amplification by convergence. Brandes and Ziegler (1993) found that tilting of perturbation horizontal vorticity associated with the MCS disturbance itself is another potentially

vorticity of at least 1–2 x 10^{-4} s^{-1} seen in the synoptic charts (cf. Fig. 3), the convergence of air at midlevels into the trailing stratiform region implies a vorticity amplification rate of at least 8–10 –10^{-4} s^{-1} day^{-1}. This is comparable to but slightly smaller than the convergence generation rate calculated by Brandes and Ziegler (1993) of 15–20 x 10^{-4} s^{-1} day^{-1} based on high-density soundings enveloping another Oklahoma MCS with an embedded vortex (the 7–8 May 1985 PRESTORM case). In the absence of turbulent energy dissipation or other forces, this effect would act to nearly triple the cyclonic vorticity in the trailing stratiform region over a 1-day period. This agrees with previous observational evidence of midlevel amplification of vertical vorticity by mesoscale convergence (e.g., Verlinde and Cotton 1990; Johnson and Bartels 1992; Brandes and Ziegler 1993), although its relative importance varies from case to case.

The second important generation mechanism expressed in Eq. (1) is twisting of horizontal vorticity by differential vertical motion. The Norman, Oklahoma, sounding taken at 0000 UTC 8 May (Fig. 11) provides an estimate of the ambient shear ahead of the developing bow echo. Above the boundary layer, most of the ambient shear is associated with increasing westerly winds up to about 5 km. The westerly shear $\partial u/\partial z$ was about 4 x 10^{-3} s^{-1}, so in the presence of north–south vertical motion gradients ($\partial w/\partial z > 0$) twisting would contribute to generation of cyclonic vorticity. Figure 10 shows that the region near the apex of the bow along the axis of the rear inflow jet was dominated by descent below about 6.5 km. The echo-free notch described in section 3 implies locally strong descent,

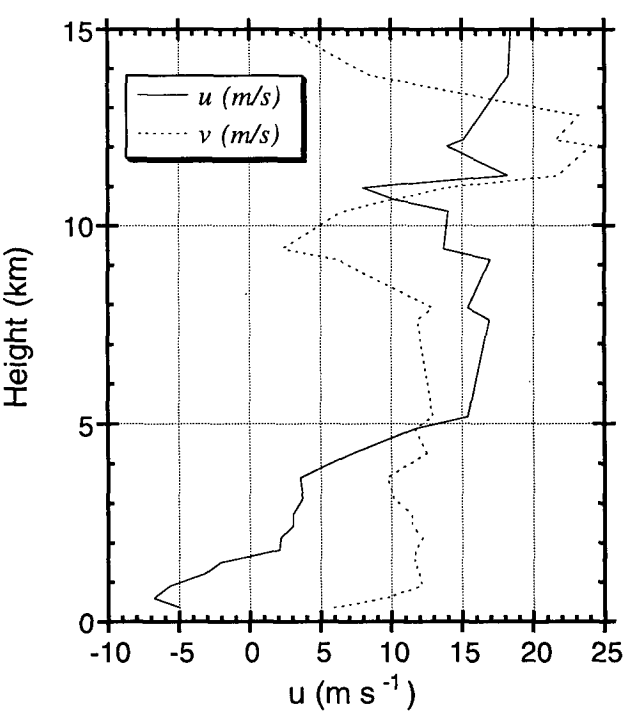

FIG. 11. East–west (u) and north–south (v) winds as a function of altitude from the 0000 UTC 8 May 1991 sounding at Norman, Oklahoma (OUN), ahead of the convective line.

important effect. Within the sampled trailing portion north of the rear-inflow jet axis of the 23 May bow-echo MCS, vertical shear displayed was partly expressed as $\partial v/\partial z > 0$ owing to a tendency for increasing southerly-component flow with height. In the presence of $\partial w/\partial x < 0$, which would be expected across the west edge of the stratiform rain area and collocated mesoscale downdraft, this mechanism could locally enhance generation of cyclonic vertical vorticity. Estimates of these terms derived from the airborne Doppler analysis ($\partial w/\partial z \sim 3 \times 10^{-3}\ s^{-1}$, $\partial w/\partial x \sim -2 \times 10^{-6}\ s^{-1}$) yield a contribution of $\sim 6 \times 10^{-4}\ s^{-1}\ day^{-1}$, for a total twisting generation rate of $\sim 13\ 10\ s^{-1}\ day^{-1}$. Brandes and Ziegler (1993) found twisting rate values of $\sim 10\text{–}15 \times 10^{-4}\ s^{-1}\ day^{-1}$ in the trailing stratiform region based on mesonetwork soundings. In view of cumulative observational and numerical evidence, it seems reasonable to conclude that the mesovortex in the trailing stratiform region of the 8 May MCS originated in association with intense convective updrafts along the convective line and was subsequently amplified/maintained by interaction of a locally intense mesoscale downdraft (descending rear-inflow jet) and some combination of the larger-scale ambient and locally perturbed vertical shear. Figure 12 schematically illustrates the arrangement of circulation features thought to be present in the mature 8 May 1991 bow-echo MCS.

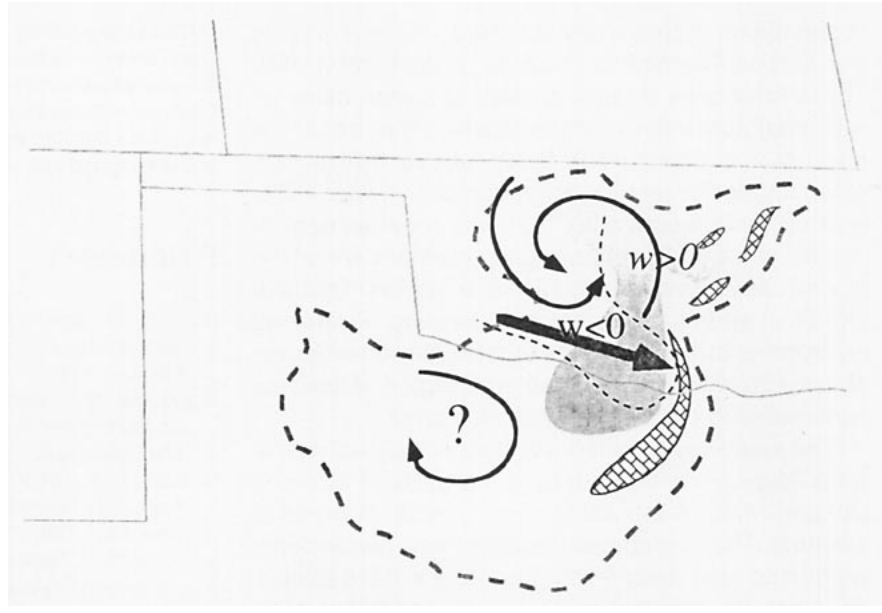

FIG. 12. Schematic illustration of key circulation features of the 8 May 1991 bow-echo mesoscale convective system. The hypothesized pattern of mesoscale vertical motion (w) is indicated. The axis of descending rear inflow is shown by the long arrow, with the counterrotating vortices shown north and south of this axis. Region of precipitation from stratiform and convective cells is depicted by the shaded region. The existence of the southern anticyclonic vortex is speculative since no airborne Doppler radar data were obtained south of the Red River in Texas.

While the available observations documented only a single (cyclonic) gyre within the northern part of the 8 May MCS, recall that simulations by Weisman (1992) showed a vortex *pair* of the sort sketched in Fig. 12. In principle, in an equatorial atmosphere devoid of large-scale vertical vorticity ($\zeta = f = 0$), there would be no reason to expect one member of the pair to dominate its counterpart. In actuality, the presence of considerable background environmental vorticity (recall this system developed near the axis of a shortwave trough) would make the spinup of the southern anticyclonic vortex difficult, since the convergence mechanism would oppose the twisting mechanism. Moreover, at Oklahoma's latitude (~35°N), convergence acting on planetary vorticity further favors the cyclonic member of the pair. Previous studies have almost exclusively documented the presence of *cyclonic* vortices (e.g., Bartels and Maddox 1991), indicative of this dominance. The existence of a double vortex structure cannot be confirmed in the present case due to limitations of the P-3 flight track coverage. One possible indication of a southern anticyclonic member is the storm's highly symmetric cloud-top temperature pattern, seen in the 0530 UTC infrared satellite image in the cover figure. As illustrated by Rutledge et al. (1988), localized erosion of the trailing anvil cloud (identified in this case by relatively warm temperatures over southwest Oklahoma) identifies the axis of the descending rear-inflow jet (cf. Fig. 12). This feature is flanked by two protruding lobes of colder cloud: one to the north positioned directly above the well-observed cyclonic mesovortex, and one to the south, which may correspond to a mirror-image anticyclone over the southeast Texas Panhandle. Future field programs should emphasize flight paths that encompass the full north–south extent of such systems.

5. Summary and conclusions

A preliminary analysis of airborne Doppler radar observations taken in a "bow-echo" MCS reveal structures previously seen or hypothesized on the basis of

observations of these systems (e.g., Fujita 1978) as well as recent numerical simulations (Weisman 1992). These structures include an elevated rear-inflow jet with maximum velocity immediately to the rear of the apex of the bow and 2–3 km above the ground extending to the leading edge convective line, a distinct cyclonic mesovortex that was most evident at middle levels (2–3 km) trailing the northern end of the bowed convective line, and a "wake" region of subsiding air. It seems likely that both twisting of ambient environmental shear and the mesoscale convergence of air into the trailing stratiform region downdraft contributed to development of this vortex.

The relatively detailed yet horizontally extensive wind fields presented attest to the utility of airborne Doppler radar in the study of mesoscale convective systems. The aircraft can map the three-dimensional winds and reflectivity fields (the likely X-band attenuation notwithstanding) in a relatively short time interval. Due to the limitations of antenna scanning rate and the airspeed of the P-3, the horizontal data spacing is limited to ~1.5 km (scanning toward both sides of the aircraft's track) or ~750 m (scanning toward only one side). A technological leap will be afforded by the ELDORA (Electra Doppler Radar) rapid-scan airborne radar developed at NCAR. Improved antenna and transmitter design (e.g., simultaneous transmission of two separate radar beams, one forward and one aft looking with each beam transmitting up to five frequencies) will allow for a two- to threefold increase in the antenna scan rate compared to the P-3, resulting in a three- to sixfold increase in horizontal data density without restricting coverage to one side of the track. A new scanning technique has been devised that involves coordinated flight tracks between two Doppler-equipped P-3 aircraft to allow for four independent radial velocity observations at every point a three-dimensional volume (Jorgensen et al. 1992). These data will allow for an overdetermined triple-Doppler solution for the winds. Owing to more direct observation of vertical hydrometeor motions, this technique should result in a two- to threefold decrease in the expected uncertainty of vertical air motion. This approach was used extensively during TOGA COARE using both P-3 aircraft and the ELDORA.

Acknowledgments. We wish to acknowledge the efforts of the flight crew members of the P-3 aircraft from NOAA's Office of Aircraft Operations in Miami, Florida. Their dedication and enthusiastic participation in COPS-91 made the collection of data in or near hazardous weather conditions possible, especially Jack Parrish (AOC project manager), Howard Ticknor (aircraft commander), Phil Kennedy (chief pilot), Jim Roles (data systems engineer), and A. Barry Damiano (flight director). The authors benefited from discussions with Morris Weisman, Diana Bartels, Conrad Ziegler, and Edward Brandes. Robert Hueftle was instrumental in development of the Doppler editing, wind syntheses, and display software, and David Johnson edited much of the P-3 Doppler radar data. The manuscript was substantially improved through reviews provided by David Stensrud and Harold Brooks. The radar reflectivity composite maps from the National Weather Service WSR-57 network were prepared by the WSI Corporation.

References

Bartels, D. L., and R. A. Maddox, 1991: Midlevel cyclonic vortices generated by mesoscale convective systems. *Mon. Wea. Rev.*, **119,** 104–118.

Biggerstaff, M. I., and R. A. Houze, Jr., 1991: Midlevel vorticity structure of the 10–11 June 1985 squall line. *Mon. Wea. Rev.*, **119,** 3066–3079.

Brandes, E. A., 1990: Evolution and structure of the 6–7 May 1985 mesoscale convective system and associated vortex. *Mon. Wea. Rev.*, **118,** 109–127.

——, and C. L. Ziegler, 1993: Mesoscale downdraft influences on vertical vorticity in a mature mesoscale convective system. *Mon. Wea. Rev.*, **121,** 1337–1353.

Burgess, D. W., and B. F. Smull, 1990: Doppler radar observations of a bow echo associated with a long-track severe windstorm. Preprints, *14th Conference on Severe Local Storms,* Kananaskis Park, Amer. Meteor. Soc., 203–208.

Davies-Jones, R. P., 1984: Streamwise vorticity: The origin of updraft rotation in supercell storms. *J. Atmos. Sci.*, **41,** 2991–3006.

Frush, C. L., P. H. Hildebrand, and C. Walther, 1986: The NCAR airborne Doppler radar. Part II: System design considerations. Preprints, *23d Conf. on Radar Meteorology,* Snowmass, Colorado, Amer. Meteor. Soc., 151–154.

Fujita, T. T., 1978: *Manual of Downburst Identification for Project NIMROD.* Satellite and Mesometeorology Research Paper No. 156, Dept. of Geophysical Science, Univ. of Chicago, 104 pp.

Hane, C. E., C. L. Ziegler, and H. B. Bluestein, 1993: Investigation of the dryline and convective storms initiated along the dryline: Field experiments during COPS-91. *Bull. Amer. Meteor. Soc.*, **74,** 2133–2145.

Hildebrand, P. H., 1989: Airborne Doppler radar accuracy. Preprints, *24th Conf. on Radar Meteorology,* Tallahassee, Florida, Amer. Meteor. Soc., 585–588.

Houze, Jr., R. A., S. A. Rutledge, M. I. Biggerstaff, and B. F. Smull, 1989: Interpretation of Doppler weather radar displays of midlatitude mesoscale convective systems. *Bull. Amer. Meteor. Soc.*, **70,** 608–619.

Johns, R. H., and W. D. Hirt, 1987: Derechos: Widespread convectively induced windstorms. *Wea. Forecasting,* **2,** 32–49.

——, K. W. Howard, and R. A. Maddox, 1990: Conditions associated with long-lived derechos—An examination of the large-scale environment. Preprints, *14th Conference on Severe Local Storms,* Kananaskis Park, Amer. Meteor. Soc., 408–412.

Johnson, and D. L. Bartels, 1992: Circulations associated with a mature-to-decaying midlatitude mesoscale convective system. Part II: Upper-level features. *Mon. Wea. Rev.*, **120,** 1301–1320.

——, R. H., S. Chen, and J. J. Toth, 1989: Circulations associated with a mature-to-decaying midlatitude mesoscale convective system. Part I: Surface features—heat bursts and mesolow development. *Mon. Wea. Rev.*, **117,** 942–959.

Jorgensen, and J. D. DuGranrut, 1991: A dual-beam technique for deriving wind fields from airborne Doppler radar. Preprints, *25th International Radar Meteorology Conf.,* Paris, France, Amer. Meteor. Soc., 458–461.

——, D. P., P. H. Hildebrand, and C. L. Frush, 1983: Feasibility test

of an airborne pulse-Doppler meteorological radar. *J. Climate Appl. Meteor.*, **22,** 744–757.

——, T. Matejka, and B. F. Smull, 1992: Multi-beam techniques for deriving wind fields from airborne Doppler radars. *Specialty Meeting on Airborne Radars and Lidars,* Toulouse, France, 33–40.

Marshall, T. C., and W. D. Rust, 1993: Two types of vertical electrical structure in stratiform precipitation regions of mesoscale convective systems. *Bull. Amer. Meteor. Soc.*, **74,** 2159–2170.

O'Brien, J. J., 1970: Alternative solution to the classical vertical velocity problem. *J. Appl. Meteor.*, **9,** 197–203.

Przybylinski, R. W., and W. J. Gery, 1983: The reliability of the bow echo as an important severe weather signature. Preprints, *13th Conf. on Severe Local Storms,* Tulsa, Oklahoma, Amer. Meteor. Soc., 270–273.

Rotunno, R., and J. B. Klemp, 1985: On the rotation and propagation of simulated supercell thunderstorms. *J. Atmos. Sci.*, **42,** 271–292.

Rutledge, S. A., R. A. Houze, Jr., M. I. Biggerstaff, and T. J. Matejka, 1988: The Oklahoma–Kansas mesoscale convective system of 10–11 June 1985: Precipitation structure and single-Doppler radar analysis. *Mon. Wea. Rev.*, **116,** 1409–1430.

Schmidt, J. M., and W. R. Cotton, 1989: A high plains squall line associated with severe surface winds. *J. Atmos. Sci.*, **46,** 281–302.

Smull, B. F., and R. A. Houze, Jr., 1985: A midlatitude squall line with a trailing region of stratiform rain: Radar and satellite observations. *Mon. Wea. Rev.*, **113,** 117–133.

Verlinde, J., and W. R. Cotton, 1990: A mesoscale vortex couplet observed in the trailing anvil of a multicellular convective complex. *Mon. Wea. Rev.*, **118,** 993–1010.

Weisman, M. L., 1992: The genesis of severe, long-lived bow echoes. *J. Atmos. Sci.*, **50,** 645–670.

Zhang, D.-L., K. Gao, and D. B. Parsons, 1989: Numerical simulations of an intense squall line during 10–11 June 1985 PRESTORM. Part I: Model verification. *Mon. Wea. Rev.*, **117,** 960–994.